HHS Public Access

Author manuscript

Mol Genet Metab. Author manuscript; available in PMC 2017 May 01.

Published in final edited form as:

Mol Genet Metab. 2016 May ; 118(1): 41–54. doi:10.1016/j.ymgme.2016.03.003.

Integrated analysis of proteome and transcriptome changes in the mucopolysaccharidosis type VII mouse hippocampus

Michael K. Parente[1,¶], **Ramona Rozen**[1,¶,#], **Steven H. Seeholzer**[1], and **John H. Wolfe**[1,2]

[1]Research Institute of the Children's Hospital of Philadelphia, Philadelphia, PA 19104. USA

[2]W. F. Goodman Center for Comparative Medical Genetics, School of Veterinary Medicine, and Department of Pediatrics, Perelman School of Medicine, University of Pennsylvania, Philadelphia, PA, 19104 USA

Abstract

Mucopolysaccharidosis type VII (MPS VII) is a lysosomal storage disease caused by the deficiency of β-glucuronidase. In this study, we compared the changes relative to normal littermates in the proteome and transcriptome of the hippocampus in the C57Bl/6 mouse model of MPS VII, which has well-documented histopathological and neurodegenerative changes. A completely different set of significant changes between normal and MPS VII littermates were found in each assay. Nevertheless, the functional annotation terms generated by the two methods showed agreement in many of the processes, which also corresponded to known pathology associated with the disease. Additionally, assay-specific changes were found, which in the proteomic analysis included mitochondria, energy generation, and cytoskeletal differences in the mutant, while the transcriptome differences included immune, vesicular, and extracellular matrix changes. In addition, the transcriptomic changes in the mutant hippocampus were concordant with those in a MPS VII mouse caused by the same mutation but on a different background inbred strain.

Keywords

mucopolysaccharidosis type VII; MPS VII; lysosomal storage disease; transcriptome; proteomic analysis; mitochondria; β-glucuronidase; GUSB; neurodegeneration; hippocampus

1. Introduction

Mucopolysaccharidosis VII (MPS VII) is a monogenic disease caused by the lack of the enzyme β-glucuronidase (GUSB) and is known to affect intellectual abilities [1, 2].

*Corresponding author: Dr. J.H. Wolfe, 502 ARC East, Children's Hospital of Philadelphia, 3615 Civic Center Blvd, Philadelphia, PA 19104, USA. jhwolfe@vet.upenn.edu.

¶Co-first authors who contributed equally to the work.

#Current address: POCARED Diagnostics Ltd., Rehovot, Israel

Lysosomal storage lesions, the hallmark of the disease, and neurodegeneration are present in the hippocampus, which has been implicated in the disease [3-6]. However, the mechanisms by which these lesions lead to neurodegeneration are not known. Proteomics and transcriptomics have both been used to analyze molecular changes associated with disease. Proteome and transcriptome analyses have also been shown to complement each other in areas of overlap and extend the range of findings because of differences in methodology [7].

Transcriptomic analysis of MPS VII versus normal littermate mice on a C3H background has shown changes in pathways and processes common to all regions of the brain, as well as some region-specific alterations [8]. To further assess the changes associated with the MPS VII brain, the present study directly compared proteomics and transcriptomic analyses in the hippocampus from the MPS VII mouse on the C57Bl/6 (B6) strain background in which neurodegeneration has been studied [3, 9, 10]. The combined results of the proteome and transcriptome changes were in functional categories consistent with many of the known histopathology findings [3, 9, 10]. The analyses extended findings of pathological alterations in some non-overlapping areas and provided information on the molecular manifestation of MPS VII disease between strains of mice.

2. Materials and Methods

2.1 Animals

All animal procedures were performed according to protocols approved by the IACUC (Institutional Animal Care and Use Committee) of the Children's Hospital of Philadelphia (CHOP). MPS VII mice and normal controls were generated from the carrier strain B6.C-H2-Kbm1 /ByBir-Gusb mps/+/J [9] and were maintained in our breeding colony through carrier-carrier brother-sister mating. Identification of the MPS VII-affected mice was verified by PCR genotyping, as described previously [10]. Carriers were used for the normal animals and they have been shown to be equivalent to the wild type [8]. Four normal and four MPS VII animals 6 months of age were used for the transcriptomics assay. For the proteomics analysis, three normal and three MPS VII mice age matched to those used for the transcriptome assay were used.

2.2 Micro-dissection of brains

The mice were anesthetized with ketamine/xylazine and the brains were removed and placed immediately on ice. The hemispheres were separated along the medial longitudinal fissure and the hippocampi were dissected out separately from each hemisphere based on anatomical boundaries, as described in [8]. The pieces were immediately frozen in liquid nitrogen and stored at -80 C until used for RNA or protein isolation.

2.3 Protein isolation and analysis

2.3.1Protein extraction and trypsin hydrolysis—Frozen mouse hippocampi of 3 normal and 3 MPS VII mice were thawed in 0.3% SDS, 50mM Tris.HCl, pH 7.8, 0.5 mM MgCl2 (1 mL/50mg wet tissue) and disrupted in a small Dounce homogenizer. The mixture was heated for 5 min at 95C, cooled to room temperature and treated with benzonase to reduce viscosity by hydrolyzing nucleic acids. After centrifugation, a small aliquot of the

clear supernatant was reserved for protein assay and the proteins were precipitated from the remainder by adding 20 ug linear polyacrylamide and 5 volumes of acetone and storing at -20C for two hours to overnight. The protein pellet was dissolved in 1× LDS sample buffer (Invitrogen), and resolved on NuPAGE 10% Bis-Tris gels (Invitrogen, Carlsbad, CA) by electrophoresis in MOPS running buffer until the dye front reached ∼3 cm. Proteins were visualized by staining for 10 min with colloidal Coomassie blue and each lane was cut into uniform (2 mm) slices using a MEF-1.5 Gel Cutter (The Gel Company, San Francisco, CA). Individual gel slices were cut into 1 mm cubes, destained, reduced with dithiothreitol, alkylated with iodoacetamide and hydrolyzed with trypsin as previously described [11].

2.3.2 LC-MS/MS analysis—Peptide digests were loaded directly onto a C_{18} capillary column (75 um × 100 mm; New Objective Proteoprep 2) isocratically in 2% Acetonitrile/ 0.1%FA at a flow rate of 1 uL per minute using an Eksigent 2D LC system. A linear gradient was then initiated at a flow rate of 300 nL per minute (3% - 40%B over 42 minutes; 40% - 100%B over 3 minutes; then 5 minutes at 100% B). Buffer A was 0.1% FA and Buffer B was 80% Acetonitrile/0.1%FA. Mass spectrometry was performed on a Thermo-Finnegan LTQ mass spectrometer in a data-dependent fashion as peptides were eluted off of the capillary column. A top 5 method was performed in which one survey scan was followed by MS/MS analysis of the 5 most intense ions. MS and MSn thresholds were set to 1500 and 500, respectively. A mass range of 300 – 1800 was implemented for all runs. A repeat count of 3 was selected such that after 3 MS/MS repeats this ion was placed onto an exclusion list for 0.5 minutes. An exclusion window was set to 0.5 below and 1.5 above the target m/z. MS/MS experiments were performed with an isolation width of 2, collision energy of 35, activation Q = 0.25, and an activation time of 30 msec.

2.3.3 Analysis of MS/MS data and database searching—Raw files were searched against the mouse-specific component of the Swiss-Prot database (fasta file created 24 March, 2009) using SEQUEST (Sorcerer2 platform, SageN) search engine to identify peptide MS2 spectral matches. Two missed cleavages were allowed. A fixed modification of S-carbamidomethylation for cysteine, and variable modification for methionine oxidation were used. A precursor mass window of 1.2 and a fragment tolerance of 0.7 Da were utilized for all ion trap–based searches. False discovery rate at the peptide and protein level was controlled using the Peptide Prophet and Protein Prophet algorithms [12, 13] as implemented in the Trans Proteomic Pipeline (TPP v4.0 JETSTREAM rev 2, Build 200902031524, Linux).

2.3.4 APEX quantification of LC-MS/MS datasets—APEX quantification of mouse brain proteins was performed using the APEX Quantitative Proteomics Tool [14] v.1.1 as described previously [15]. Using the interact.prot.xml file from TPP analysis, a training dataset ARFF file was constructed from the 100 most frequently identified proteins. The random forest classifier algorithm was applied to the training set and then to all the *in silico*-generated tryptic peptides from the mouse fasta file to allow calculation of the complete set of mouse protein observability index (Oi) values. Apex abundances for all the observed mouse brain proteins were finally calculated using the intertact.prot.xml files generated for each experiment by the TPP analysis of the SEQUEST search results.

2.4 RNA isolation and microarray analysis

2.4.1 RNA isolation—Total RNA was isolated from the right hippocampus. Frozen tissue was placed into TRIzol (Invitrogen) at 1 ml per sample and homogenized (Pellet Pestle Motor - Kontes, VWR) at maximum speed for 20-40 Sec. The RNA was further purified using the RNeasy Lipid Tissue mini kit (Qiagen) according to manufacturer's instructions. Total RNA quality was assessed by measuring the $A_{260/280}$ ratio on a NanoDrop ND-1000 spectrophotometer (Thermo Scientific). RNA integrity was verified by visualization of the 28S and 18S ribosomal rRNA bands, with no presence of smear, using a denaturing TAE-agarose gel.

2.4.2 Microarrays—1 μg RNA was used to prepare biotinylated aRNA samples using the MessageAMP II-biotin Enhanced Signal Round aRNA Amplification Kit (Ambion). Reverse transcription, in vitro transcription and fragmentation were performed according to manufacturer's instructions (Ambion). Samples of 10 μg aRNA were hybridized on Affymetrix mouse genome 430A 2.0 Gene Chips containing 22,690 oligonucleotide probe sets (www.affymetrix.com). Hybridization, staining and washing were performed on an Affymetrix Fluidics Station 400 at the Children's Hospital of Philadelphia Nucleic Acid Core facility according to Affymetrix protocols. Scanning was performed using the Affymetrix Gene Chip Scanner 3000 controlled by a GeneChip Operating software 1.4 (GCOS, Affymetrix).

2.4.3 Data normalization and analysis—Raw microarray image files were processed using the Affymetrix GCOS 1.4 software to calculate individual probe cell intensity data and generate CEL data files. The CEL files were imported into Partek Genomics Suite (v6.5, Partek Inc., St. Louis, MO) where RMA normalization was applied.

2.5 Statistics

2.5.1 Proteomics—Partek Genomics Suite (v6.5, Partek, Inc., St. Louis, MO) was used for statistical analysis. Proteins were considered significantly different at the non-corrected level of $p<0.05$. The software calculates p-values when one group has a protein detected in only one animal and the other group has that protein detected in multiple animals by assuming the variance of the more complete group. Statistical analysis of proteins undetected in one group but detected in all three animals of the other group and the issue of non-detected proteins is discussed in the results section.

2.5.2 Transcriptomics—Significant Analysis of Microarray (SAM) was used for the transcriptomics significance calculation because its false discovery rate calculation is optimized for microarray analysis [16]. Gene transcription was considered significantly different at the level of $q<0.05$ with a >1.5 fold change.

2.5.3 Statistics abbreviations—p-value (small p), probability test value for significance; P-value (large P), strength of association in Spearman's Rank Correlation [17] or enrichment value in DAVID analysis [18]; q-value, probability test with false discovery rate calculation [19].

2.5.4 Proteomic/transcriptomic comparison—UniProt protein accession numbers (www.uniprot.org) and Affymetrix probe IDs were converted to DAVID IDs (http://david.abcc.ncifcrf.gov/) for comparison.

2.5.5 Spearman rank order—Two-tailed Spearman rank order was calculated using the online calculator provided by http://www.vassarstats.net [17].

2.5.6 Functional annotation analysis—The significantly changed proteins ($p<0.05$) and gene transcription changes ($q<0.05$) were analyzed using Database for Annotation, Visualization and Integrated Discovery v6.7 (DAVID) (http://david.abcc.ncifcrf.gov) [20] for Gene Ontology (GO) terms [21] using the mus musculis background, Kyoto Encyclopedia of Genes and Genomes (KEGG) [22] and other database enrichment and functional clustering, or from literature-search generated gene lists as described in the results section. The Euler diagram of proportionality was generated by EulerAPE from http://www.eulerdiagrams.org/eulerAPE/#Downloads [23]. The functional groups used terms that defined cell processes or pathways and did not include terms that were broadly representative of all cells, such as cell membrane, cytoplasm or nucleus.

3. Results

3.1 Proteomic detection

We chose to analyze a subregion of the brain for proteomic analysis since a previous transcriptome study showed there were significant differences between brain regions in the alterations caused by the disease [8]. The hippocampus was selected because it has been studied in this model both for histopathology [3, 9, 10, 24] and behavioral abnormalities [4-6, 25]. The B6 strain of MPS VII mouse was chosen due to the severity of disease in order to maximize the differences between normal and MPS VII hippocampi [24]. The disease features in the C3H strain are essentially the same as the B6 background at the end-stage, but C3H has a significantly longer lifespan [24].

A total of 3268 independent proteins were detected in the hippocampus among all of the mice (Supplemental Data 1.xls), but not all proteins were detected in every animal, which is a common finding in gel based mass spectrometry analyses [26-28]. A total of 2989 unique proteins were detected among the normal mice and 2686 among the MPS VII mice. Significant differences between genotypes were found in 189 proteins ($p<0.05$).

A second group of protein changes were those detected in all mice of one genotype but in none of the other genotype, but a p-value and fold change could not be calculated because the actual level of the undetected group was unknown. The level of a protein that was not detected in one genotype was hypothesized to be less than the level in the genotype where the same protein was detected in all animals, and thus likely to represent a meaningful biological difference. To evaluate this assumption and determine if those protein changes could be included in the analysis, we used a “likelihood” approach that has been applied to non-detected proteins in proteomic analysis [28]. The average level for all the proteins detected in all three animals was compared to the average of those detected in any two animals and to the average of those detected in just one animal within the phenotype groups.

The average level for all of the proteins detected in all three animals was 5-fold greater than the average level for those detected in just two animals ($p<0.001$) and was 10 fold greater than the average of all the proteins detected in any one animal ($p<0.0001$) (Supplemental Data 2.xlsx). This is consistent with the finding that proteomics favors the detection of the more abundant proteins [26, 27] and conversely, that non-detected proteins are likely to be associated with lower protein levels.

On the basis of this, it was concluded that the level of a protein not detected in any animal of one genotype was likely lower than when it was detected in all 3 of the other genotype. This group included 68 proteins, with 59 in the normal animals and 9 in the mutants. and were included in the analysis of mutant vs normal with only a direction of change (arrows in tables) assigned without p-value or fold change. This likelihood basis was also used to remove 12 outliers (6 increases, 6 decreases) where proteins detected in only one animal of a genotype had a higher level than the average for the other genotype with multiple detections. Thus the total number of proteins included in the analysis of changes in the MPS VII hippocampus was 245 (7% of the detected proteins) (Table 1). Of these, 174 proteins were decreased (71%) and 71 were increased (29%) in the MPS VII brain. These were then analyzed for changes in functional annotation terms, which require multiple changes per term, rather than individual gene products.

3.2 Proteomic annotation enrichment analysis

The functional annotation terms were generated for the protein changes with DAVID enrichment analysis (http://david.abcc.ncifcrf.gov/) using the same analytical approach as our previous transcriptome analysis [8]. A minimum of 3 significantly changed proteins were required per annotation term. A total of 743 unique terms were generated (Supplemental Data 3.pdf) and related terms were consolidated into larger functional categories representing related biological processes (Table 2).

The largest percentage of total detected proteins (14%) was the mitochondrial functional category, which included 42% of the mitochondrial-related genes in the MitoCarta database (http://www.broadinstitute.org/pubs/MitoCarta/) (Table 3). Among all the significantly changed proteins in the MPS VII brain, 80 (about 1/3) belonged to the mitochondrial category. Since mitochondrial protein alterations implicate the cellular energy generating system, a comparison to Palmfeldt's mitochondrial sub-categories list [29] (Table 4) showed: 1) the proteins associated with the canonical citric acid cycle enzymes were all increased (2 significantly), except alpha-ketoglutarate dehydrogenase (Oghd) which was significantly reduced; and 2) all 11 significant changes in the mitochondria localized respiratory chain were decreased (complex 2 is a component of the citric acid cycle and was grouped with the citric acid cycle proteins [30]). In addition, although cytosolic, 87% of the energy generating glycolytic enzymes were also increased, two significantly (Gpi and Aldoc) (Table 5). The increases in the citric acid cycle and glycolytic enzymes were disproportionate to the decreases in the overall proteome (60%), the mitochondrial proteins (65%), and the respiratory chain associated proteins (78%), which suggests an alteration in energy generation.

The greatest number of functional terms (62) were in the cytoskeleton category, which were generated from 66 significantly changed proteins (Table 6). Most of these were decreased in the mutant (74%), with all classes of motor proteins (kinesins, dyneins, and myosins) showing significant reductions in MPS VII. Also of interest are several protein changes associated with the cytoskeletal-membrane linking ankyrin proteins such as: Shank3 whose superfamily Shank proteins play a role in synapse formation and dendritic spine maturation [31] and Asap1, Asap2, Agap2, and Ankfy1, which are all involved with endocytosis.

3.3 Transcriptomic annotation enrichment analysis

A transcriptome analysis of BL6 MPS VII versus normal hippocampus was performed to compare to the proteomic results (Supplemental Data 4.xlsx). The number of mice was chosen to be in the same range as the proteome cohort, which was limited due to the nature of the assay. This experiment was also designed to focus on the most prominent differences between the normal and diseased brains. The transcriptomic data was analyzed using the Significance Analysis of Microarrays (SAM) [16] program. Significant differences ($q< 0.05$ and fold >1.5) were found in the expression of 81 probe sets accounting for 69 genes, of which 66 were up-regulated and 3 were down-regulated (Table 7).

DAVID functional annotation terms were generated from the list of significantly altered gene transcript changes in the same manner as the proteome. This generated 229 unique annotation terms which grouped into 29 clusters (Supplemental Data 5.pdf). As with the proteome, the gene expression changes and terms were compared to the functional categories previously assigned in the analysis of the C3H mouse [8]. Of the significant gene expression changes in the BL6 mouse in the present study, 40 of the changes (58%) were the same as in the C3H mouse and 100% of the shared changes were in the same direction (Figure 1). Furthermore, 94% of the annotation terms generated from this BL6 mouse study were present in the terms generated in the C3H mouse hippocampus [8]. Thus the overall pattern of altered processes between strains was highly consistent, which also correlates with clinical and pathological findings [3]. Functional categories were assigned similarly to the proteomic assignments (Table 2). Four of the categories generated by the proteome (protein modification, neural disease, ubiquitin and cell cycle) were not represented in the BL6 transcriptome (Table 2).

3.4 Comparison of Proteomic and Transcriptomic analyses

The results of the two assays were first compared using the UniProt tissue annotation enrichment tool [32], which ascertains if a list of genes or proteins is statistically over-represented (enriched) for specific tissue annotations, as a method of validating the detected proteins. There was a high degree of enrichment for the tissue annotation terms “brain” ($P\approx10^{-187}$), “hippocampus” ($P\approx10^{-174}$), and “brain cortex” ($P\approx10^{-114}$) (Supplemental Data 6.pdf). To ascertain that systematic database bias [29] was not responsible for this result, and since mitochondrial proteins were the largest category of proteins detected, the entire MitoCarta list was submitted and the enrichment score for “hippocampus” and “brain” were much lower ($P\approx10^{-23}$, $P\approx10^{-2}$ respectively).

Tissue annotation of the transcriptome was accomplished by analyzing the 3200 highest expressing probe sets which was about 12% of the probes on the chipset and about the number of proteins detected. This also showed that “brain,” “hippocampus,” and “brain cortex” were enriched at $P \approx 10^{-100}$ (Supplemental Data 6.pdf). To test for systematic bias, 2 random sets of 3200 probes were analyzed which showed that the top tissue annotations were non-neural (Supplemental Data 6.pdf) and the top neural tissue, “hippocampus,” was enriched only to $P \approx 10^{-9}$. The proteomic and transcriptomic tissue annotations were compared by Spearman rank order correlation and there was greater correlation to each other than to the random probe sets.

Since we did not find an analysis of this type in the literature, we explored what would happen using an iterative analysis of varying numbers of top expressing probes. With up to 200 probes, “hippocampus” was the top annotation, with “brain” second. Between 200-3200 probes, the term “brain” was the top annotation followed by “hippocampus.” At more than 3200 terms, the annotation for “hippocampus” began to decrease, the annotation for “brain” began to level off, and miscellaneous other annotations began to rapidly rise (Figure 2).

One of the problems with integrated proteomic and transcriptomic analysis using the methods here is that many probes present on the microarray are not detected in the proteome and not all of the detected proteins have corresponding probes on the microarray. To compare the results of the two methods we converted the Uniprot Identifiers and the Affymetrix probe set IDs to DAVID ID numbers using the DAVID program. Of the detected proteins, 86% had a matching probeset in the microarray (cognate pairs of transcripts and proteins), which represented about one-fifth of all the microarray probes. Of the 245 proteins that were significantly different in the MPS VII brain, 82% had a cognate mRNA transcript represented on the microarray and 43 of the changed proteins were not represented in the microarray. However, the annotation terms they generated were largely redundant with the terms already found, thus their absence had little effect on the characterization of the pathologic changes. Conversely, only 10 (14%) of the 69 significant gene transcription changes had cognates among the detected proteins and none of them were changed between normal and diseased brains.

Overall, the changes in the proteome and transcriptome were in opposite directions, with 71% of the significant proteomic changes being decreases and 96% of the significant transcriptomic changes being increases. While it is known that mRNA and protein levels correlate poorly, this discrepancy was explored by examining cognate pairs from the two assays for their direction of change. When the cognate changes were filtered for successively smaller p- and q-values, they became increasingly more likely to be in the same direction (Supplemental Data 7.pdf). This is consistent with studies that have shown: 1) as noise is reduced, the direction of change is more consistent between proteins and transcripts [33]; and 2) that gross proteome and transcriptome changes can be in the opposite directions in an integrated analysis [34]. Thus, the difference in the overall directions-of-change was consistent with what others have seen.

Despite the fact that there were no mutually significant cognate changes between the two assays, 110 of the 229 transcriptomic annotation terms (48%) were among the 773

annotation terms generated in the proteomic analysis (Figure 1). The shared terms were grouped by their assigned functional categories (Table 8). Although fewer in number, the transcriptomic terms generated in the BL6 strain in the present study were very similar to those identified for the hippocampus in the C3H strain, which carries the same mutation in GUSB [8, 24]. Additionally, the proportion of transcriptome terms that were shared with the proteome was similar for both strains (Figure 1).

4. Discussion

The present study was undertaken to assess the changes associated with diseased brain tissue in a widely studied model of lysosomal storage disease, MPS VII, which is a genetic model of mental retardation. We focused the analysis on a single region because transcriptomic analysis in this model showed not only numerous changes between normal and diseased brains, but also significant differences in the changes between brain regions [8]. We chose the hippocampus because of the extensive histopathology associated with this region [3, 9, 10].

Proteomic and transcriptomic analytical methods each provide meaningful insights into the study of normal and diseased states [7]. Global changes in mRNA levels have been found to not correlate well with the translated cognate proteins [35, 36] due to post-transcriptional regulatory processes, mRNA stability, and protein stability [37-39]. Proteomic and transcriptomic analysis both give rise to noisy data, use very different experimental methodologies, which complicates comparisons [40], and can even show an overall opposite directions of change by the two assay systems [34], as we observed. Nevertheless, they are complementary in their findings [7] as we also observed.

Our long-term goal is to obtain understanding of the complex pathological processes that arise in this single gene disease affecting the CNS. However, the changes in either protein abundance or transcript expression from individual genes give an incomplete picture of the pathogenic mechanisms. In contrast, analyzing the changes for functional annotation terms and broader categories, which require multiple changes, provides a common set of descriptors for the disease-associated alterations that can occur even in the absence of cognate changes.

None of the statistically significant changes in either protein or mRNA levels between normal and MPS VII hippocampus involved the same gene product. Limited studies of non-inherited diseases have also found few overlapping changes between the two assays [41-43]. Despite this discordance, the annotation analysis of the changes implicated many of the same pathologic processes, with about a third of the functional annotation terms from the two assays being the same. A number of these terms were for processes involved in known pathology in the MPS VII brain, such as those involving the hallmark lysosome/vesicular system, neuronal functions, and inflammatory/immune processes [3, 9, 10]. Thus, functional annotation analysis implicated many of the same areas of pathology even though the specific gene products had no overlap.

While “omic” assays are unbiased for comparison within each assay system, comparisons between assay systems have biases for technological and biological reasons. For example, both assays showed changes in complement cascade components, with significantly changed mRNA levels where no protein was detected, and protein changes where no corresponding mRNA probe was available on the microarray. The complement changes are interesting in light of the fact that complement component C1q has been found to bind to and be spatially associated with chondroitin sulfate proteoglycans in another lysosomal storage disease, Niemann-Pick C [44], and chondroitin sulfate is the main storage product of MPS VII. Furthermore, complement components have a role in brain development and are altered in a number of neurodegenerative diseases [45].

Comparison of the disease changes between the two assays was constrained by the limits of the proteomic assay since most of the altered proteins had probes on the microarray chip, but only a sixth of the significantly altered mRNAs had their cognate proteins detected. For example, CD68, a prominent marker of microglia activation, was one of the most significant gene expression changes in both the Bl6 and C3H mouse, yet was not detected in the proteomic assay. Nevertheless, the protein increase is readily detectable by immunohistochemistry in the MPS VII diseased brain and is a good indicator of early neuropathology and therapeutic correction [9]. This indicates that the amount of protein needed for immunofluorescence detection of a difference is below the level needed to for detection in the proteomic assay.

Proteomic analysis is also constrained due to its detection of the more abundant proteins, such as mitochondrial and cytoskeletal proteins, which resulted in those being the majority of protein differences between the MPS VII and normal brains. Mitochondrial abnormalities have been identified in several MPS diseases [46], including accumulation of defective mitochondria through the impairment of autophagy [47] and may be responsible for the energy imbalances seen in MPS VII [48].

The proteomic changes in the major energy generating pathways are consistent with Warburg's finding of an increase in aerobic glycolysis in tumors [49], which can also occur in inflammatory conditions [50]. Evidence of this alteration in the MPS VII brain is that most of the glycolytic and citric acid cycle enzymes were increased. Furthermore, the two glycolytic enzymes that were decreased (Hk1 and Pfkp) are involved in the ATP investment phase of glycolysis and have been shown in tumor cells to consistently decrease when the other glycolytic enzymes are increased [51]. In the citric acid cycle, the only decrease was in α-ketoglutarate dehydrogenase (Ogdh), which is believed to be a regulator of flux through the citric acid cycle [52]. An impaired function of this enzyme is characteristic of several neurodegenerative diseases, where it is decreased [52]. In contrast, in the respiratory chain, all 11 of the significantly changed proteins were decreases, which have been associated with neurodegeneration [53]. Thus, the alterations in mitochondrial and other energy system proteins in the brain are consistent with altered energy balance, and thus are likely to have a role in neurodegeneration.

Despite the differences between the two assays, the overlapping annotation terms were consistent with known histopathologic alterations such as the classic lysosomal alterations,

while others suggest new directions to investigate such as the role of complement and energy generation in this monogenic disease.

Supplementary Material

Refer to Web version on PubMed Central for supplementary material.

Acknowledgments

We wish to thank T. Clarke, for technical assistance; E. Rappaport for help with microarray processing; and J. Tobias for bioinformatics advice. This work was supported by the NIH NINDS (R01-NS038690, R01-NS088667), the Ethel Foerderer Foundation; and an Intellectual and Developmental Disabilities Research Center from the NICHD (U54-HD086984).

References

1. Sly WS, Quinton BA, McAlister WH, Rimoin DL. Beta glucuronidase deficiency: report of clinical, radiologic, and biochemical features of a new mucopolysaccharidosis. J Pediatr. 1973; 82:249–257. [PubMed: 4265197]
2. Neufeld, E.; Muenzer, J. The mucopolysaccharidoses. In: Scriver, C.; Beaudet, A.; Sly, W.; Valle, D., editors. The Metabolic & Molecular Basis of Inherited Disease. McGraw-Hill; New York: 2001. p. 3421-3452.
3. Heuer GG, Passini MA, Jiang K, Parente MK, Lee VM, Trojanowski JQ, Wolfe JH. Selective neurodegeneration in murine mucopolysaccharidosis VII is progressive and reversible. Ann Neurol. 2002; 52:762–770. [PubMed: 12447930]
4. Brooks AI, Stein CS, Hughes SM, Heth J, McCray PM Jr, Sauter SL, Johnston JC, Cory-Slechta DA, Federoff HJ, Davidson BL. Functional correction of established central nervous system deficits in an animal model of lysosomal storage disease with feline immunodeficiency virus-based vectors. Proc Natl Acad Sci U S A. 2002; 99:6216–6221. [PubMed: 11959904]
5. Frisella W, O'Connor L, Vogler C, Roberts M, Walkley S, Levy B, Daly T, Sands M. Intracranial injection of recombinant adeno-associated virus improves cognitive function in a murine model of mucopolysaccharidosis type VII. Mol Ther. 2001:351–358. [PubMed: 11273777]
6. O'Connor LH, Erway LC, Vogler CA, Sly WS, Nicholes A, Grubb J, Holmberg SW, Levy B, Sands MS. Enzyme replacement therapy for murine mucopolysaccharidosis type VII leads to improvements in behavior and auditory function. J Clin Invest. 1998; 101:1394–1400. [PubMed: 9525982]
7. Zhang W, Li F, Nie L. Integrating multiple ‘omics’ analysis for microbial biology: application and methodologies. Microbiology. 2010; 156:287–301. [PubMed: 19910409]
8. Parente MK, Rozen R, Cearley CN, Wolfe JH. Dysregulation of Gene Expression in a Lysosomal Storage Disease Varies between Brain Regions Implicating Unexpected Mechanisms of Neuropathology. PLoS One. 2012; 7:e32419. [PubMed: 22403656]
9. Griffin TA, Anderson HC, Wolfe JH. Ex Vivo Gene Therapy Using Patient iPSC-Derived NSCs Reverses Pathology in the Brain of a Homologous Mouse Model. Stem Cell Reports. 2015 IN PRESS.
10. Levy B, Galvin N, Vogler C, Birkenmeier EH, Sly WS. Neuropathology of murine mucopolysaccharidosis type VII. Acta Neuropathol. 1996; 92:562–568. [PubMed: 8960313]
11. Spodik, B.; Seeholzer, SH.; Coleman, TR. Using Xenopus egg extracts to modify recombinant proteins. In: Coleman, EA., editor. Protein-Protein Interactions. Cold Spring Harbor Lab. Press; Cold Spring Harbor: 2002. p. 355-374.
12. Keller A, Nesvizhskii AI, Kolker E, Aebersold R. Empirical statistical model to estimate the accuracy of peptide identifications made by MS/MS and database search. Anal Chem. 2002; 74:5383–5392. [PubMed: 12403597]
13. Nesvizhskii AI, Keller A, Kolker E, Aebersold R. A statistical model for identifying proteins by tandem mass spectrometry. Anal Chem. 2003; 75:4646–4658. [PubMed: 14632076]

14. Braisted JC, Kuntumalla S, Vogel C, Marcotte EM, Rodrigues AR, Wang R, Huang ST, Ferlanti ES, Saeed AI, Fleischmann RD, Peterson SN, Pieper R. The APEX Quantitative Proteomics Tool: generating protein quantitation estimates from LC-MS/MS proteomics results. BMC Bioinformatics. 2008; 9:529. [PubMed: 19068132]
15. Kuntumalla S, Braisted JC, Huang ST, Parmar PP, Clark DJ, Alami H, Zhang Q, Donohue-Rolfe A, Tzipori S, Fleischmann RD, Peterson SN, Pieper R. Comparison of two label-free global quantitation methods, APEX and 2D gel electrophoresis, applied to the Shigella dysenteriae proteome. Proteome Sci. 2009; 7:22. [PubMed: 19563668]
16. Tusher VG, Tibshirani R, Chu G. Significance analysis of microarrays applied to the ionizing radiation response. Proc Natl Acad Sci U S A. 2001; 98:5116–5121. [PubMed: 11309499]
17. Lowry, R. Vassar Stats: Website for Statistical Computation. 2015. http://www.vassarstats.net/corr_rank.html
18. Gene_Ontology_Consortium. GO Enrichment Analysis. 2015. http://geneontology.org/page/go-enrichment-analysis
19. Storey JD. A direct approach to false discovery rates. J R Statist Soc B. 2002; 64:478–498.
20. Huang DW, Sherman BT, Lempicki RA. Systematic and integrative analysis of large gene lists using DAVID bioinformatics resources. Nat Protoc. 2009; 4:44–57. [PubMed: 19131956]
21. Ashburner M, Ball CA, Blake JA, Botstein D, Butler H, Cherry JM, Davis AP, Dolinski K, Dwight SS, Eppig JT, Harris MA, Hill DP, Issel-Tarver L, Kasarskis A, Lewis S, Matese JC, Richardson JE, Ringwald M, Rubin GM, Sherlock G. Gene ontology: tool for the unification of biology. The Gene Ontology Consortium. Nat Genet. 2000; 25:25–29. [PubMed: 10802651]
22. Kanehisa M, Goto S, Furumichi M, Tanabe M, Hirakawa M. KEGG for representation and analysis of molecular networks involving diseases and drugs. Nucleic AcidsRes. 2010; 38:D355–360.
23. R, P.; Chow, S. Constructing area-proportional Venn and Euler diagrams with three circles [Abstract] INRIA Rocquencourt. Euler Diagrams Workshop; Paris: 2005.
24. Casal ML, Wolfe JH. Variant clinical course of mucopolysaccharidosis type VII in two groups of mice carrying the same mutation. Lab Invest. 1998; 78:1575–1581. [PubMed: 9881957]
25. Liu W, Griffin G, Clarke T, Parente MK, Valentino RJ, Wolfe JH, Fraser NW. Bilateral single-site intracerebral injection of a nonpathogenic herpes simplex virus-1 vector decreases anxiogenic behavior MPS VII mice, Molecular therapy. Methods & clinical development. 2015; 2:14059. [PubMed: 26052529]
26. Taylor SL, Leiserowitz GS, Kim K. Accounting for undetected compounds in statistical analyses of mass spectrometry 'omic studies. Stat Appl Genet Mol Biol. 2013; 12:703–722. [PubMed: 24246290]
27. Albrecht D, Kniemeyer O, Brakhage AA, Guthke R. Missing values in gel-based proteomics. Proteomics. 2010; 10:1202–1211. [PubMed: 20077407]
28. Wood J, White IR, Cutler P. A likelihood-based approach to defining statistical significance in proteomic analysis where missing data cannot be disregarded. Signal Processing. 2004; 84:1777–1788.
29. Palmfeldt J, Vang S, Stenbroen V, Pedersen CB, Christensen JH, Bross P, Gregersen N. Mitochondrial proteomics on human fibroblasts for identification of metabolic imbalance and cellular stress. Proteome Sci. 2009; 7:20. [PubMed: 19476632]
30. Chaban Y, Boekema EJ, Dudkina NV. Structures of mitochondrial oxidative phosphorylation supercomplexes and mechanisms for their stabilisation. Biochim Biophys Acta. 2014; 1837:418–426. [PubMed: 24183696]
31. Pruitt KD, Tatusova T, Maglott DR. NCBI reference sequences (RefSeq): a curated non-redundant sequence database of genomes, transcripts and proteins. Nucleic AcidsRes. 2007; 35:D61–65.
32. UniProt_Consortium. The Universal Protein Resource (UniProt) in 2010. Nucleic Acids Res. 2010; 38:D142–148. [PubMed: 19843607]
33. Ghazalpour A, Bennett B, Petyuk VA, Orozco L, Hagopian R, Mungrue IN, Farber CR, Sinsheimer J, Kang HM, Furlotte N, Park CC, Wen PZ, Brewer H, Weitz K, Camp DG 2nd, Pan C, Yordanova R, Neuhaus I, Tilford C, Siemers N, Gargalovic P, Eskin E, Kirchgessner T, Smith DJ, Smith RD, Lusis AJ. Comparative analysis of proteome and transcriptome variation in mouse. PLoS Genet. 2011; 7:e1001393. [PubMed: 21695224]

34. Cho YE, Singh TS, Lee HC, Moon PG, Lee JE, Lee MH, Choi EC, Chen YJ, Kim SH, Baek MC. In-depth identification of pathways related to cisplatin-induced hepatotoxicity through an integrative method based on an informatics-assisted label-free protein quantitation and microarray gene expression approach. Mol Cell Proteomics. 2012; 11:M111 010884. [PubMed: 22023808]
35. Waters KM, Pounds JG, Thrall BD. Data merging for integrated microarray and proteomic analysis, Briefings. Functional Genomics And Proteomics. 2006; 5:261–272.
36. Haider S, Pal R. Integrated analysis of transcriptomic and proteomic data. Curr Genomics. 2013; 14:91–110. [PubMed: 24082820]
37. Vogel C, Marcotte EM. Calculating absolute and relative protein abundance from mass spectrometry-based protein expression data. Nat Protoc. 2008; 3:1444–1451. [PubMed: 18772871]
38. Vogel C, Marcotte EM. Insights into the regulation of protein abundance from proteomic and transcriptomic analyses. Nat RevGenet. 2012; 13:227–232.
39. Schwanhausser B, Busse D, Li N, Dittmar G, Schuchhardt J, Wolf J, Chen W, Selbach M. Global quantification of mammalian gene expression control. Nature. 2011; 473:337–342. [PubMed: 21593866]
40. Mootha VK, Bunkenborg J, Olsen JV, Hjerrild M, Wisniewski JR, Stahl E, Bolouri MS, Ray HN, Sihag S, Kamal M, Patterson N, Lander ES, Mann M. Integrated analysis of protein composition, tissue diversity, and gene regulation in mouse mitochondria. Cell. 2003; 115:629–640. [PubMed: 14651853]
41. Chin MH, Qian WJ, Wang H, Petyuk VA, Bloom JS, Sforza DM, Lacan G, Liu D, Khan AH, Cantor RM, Bigelow DJ, Melega WP, Camp DG 2nd, Smith RD, Smith DJ. Mitochondrial dysfunction, oxidative stress, and apoptosis revealed by proteomic and transcriptomic analyses of the striata in two mouse models of Parkinson's disease. J Proteome Res. 2008; 7:666–677. [PubMed: 18173235]
42. Ritter SY, Subbaiah R, Bebek G, Crish J, Scanzello CR, Krastins B, Sarracino D, Lopez MF, Crow MK, Aigner T, Goldring MB, Goldring SR, Lee DM, Gobezie R, Aliprantis AO. Proteomic analysis of synovial fluid from the osteoarthritic knee: comparison with transcriptome analyses of joint tissues. Arthritis Rheum. 2013; 65:981–992. [PubMed: 23400684]
43. Kjellqvist S, Maleki S, Olsson T, Chwastyniak M, Branca RM, Lehtio J, Pinet F, Franco-Cereceda A, Eriksson P. A combined proteomic and transcriptomic approach shows diverging molecular mechanisms in thoracic aortic aneurysm development in patients with tricuspid- and bicuspid aortic valve. Mol Cell Proteomics. 2013; 12:407–425. [PubMed: 23184916]
44. Lopez ME, Klein AD, Scott MP. Complement is dispensable for neurodegeneration in Niemann-Pick disease type C. J Neuroinflammation. 2012; 9:216. [PubMed: 22985423]
45. Stephan AH, Barres BA, Stevens B. The complement system: an unexpected role in synaptic pruning during development and disease. Annu Rev Neurosci. 2012; 35:369–389. [PubMed: 22715882]
46. Kiselyov K, Muallem S. Mitochondrial Ca2+ homeostasis in lysosomal storage diseases. Cell Calcium. 2008; 44:103–111. [PubMed: 18242695]
47. Settembre C, Fraldi A, Jahreiss L, Spampanato C, Venturi C, Medina D, de Pablo R, Tacchetti C, Rubinsztein DC, Ballabio A. A block of autophagy in lysosomal storage disorders. Hum Mol Genet. 2008; 17:119–129. [PubMed: 17913701]
48. Woloszynek JC, Coleman T, Semenkovich CF, Sands MS. Lysosomal dysfunction results in altered energy balance. J Biol Chem. 2007; 282:35765–35771. [PubMed: 17911106]
49. Warburg O. On respiratory impairment in cancer cells. Science. 1956; 124:269–270. [PubMed: 13351639]
50. Wen H, Ting JP, O'Neill LA. A role for the NLRP3 inflammasome in metabolic diseases--did Warburg miss inflammation? Nat Immunol. 2012; 13:352–357. [PubMed: 22430788]
51. Gaglio D, Metallo CM, Gameiro PA, Hiller K, Danna LS, Balestrieri C, Alberghina L, Stephanopoulos G, Chiaradonna F. Oncogenic K-Ras decouples glucose and glutamine metabolism to support cancer cell growth. Mol Syst Biol. 7:523. [PubMed: 21847114]
52. Tretter L, Adam-Vizi V. Alpha-ketoglutarate dehydrogenase: a target and generator of oxidative stress. Philos Trans R Soc Lond B Biol Sci. 2005; 360:2335–2345. [PubMed: 16321804]

53. Koopman WJ, Distelmaier F, Smeitink JA, Willems PH. OXPHOS mutations and neurodegeneration. EMBO J. 2013; 32:9–29. [PubMed: 23149385]

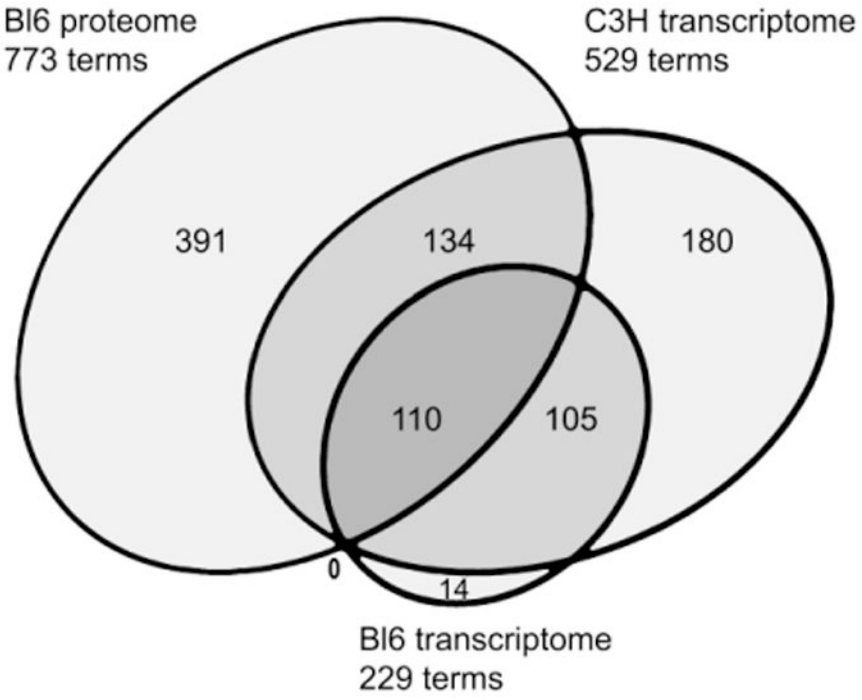

Figure 1.

Proportional Euler diagram of shared DAVID functional terms from diseased versus normal mice between Bl6 proteomic and Bl6 and C3H transcriptomic analyses.

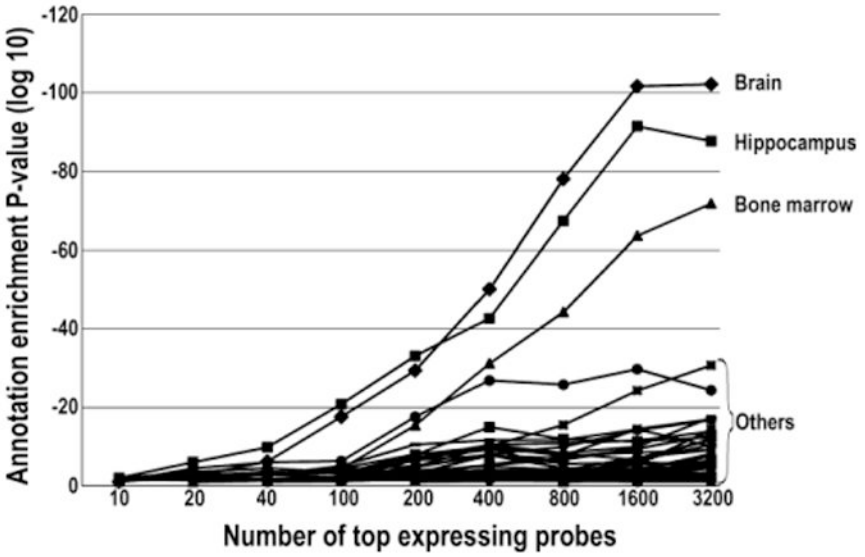

Figure 2.

Transcriptomic tissue annotation profile from increasing numbers of top expressing probes showing the ranking of tissue annotation for the top expressing probes at increasing depth.

Table 1
Proteomic changes sorted by fold change in the MPS VII hippocampus

Up and down arrows indicate direction of change when fold-change could not be calculated as discussed in the results section.

Uniprot ID	Gene Name	p-value	Fold	Description
P10922	H1f0		↑	H1 histone family, member 0
P17047	Lamp2		↑	lysosomal-associated membrane protein 2
P97441	Slc30a3		↑	solute carrier family 30 (zinc transporter), member 3
Q61035	Hars		↑	histidyl-tRNA synthetase
Q68FD9	Kiaa1549		↑	RIKEN cDNA D630045J12 gene
Q7TQ95	Lnp		↑	limb and neural patterns
Q924L1	Letmd1		↑	LETM1 domain containing 1
Q9DCP2	Slc38a3		↑	solute carrier family 38, member 3
Q9EPR4	Slc23a2		↑	solute carrier family 23 (nucleobase transporters), member 2
Q64310	Surf4	<0.001	5.73	surfeit gene 4
Q5DU25	Iqsec2	0.010	4.02	IQ motif and Sec7 domain 2
A2RT62	Fbxl16	0.016	3.65	F-box and leucine-rich repeat protein 16
P12367	Prkar2a	0.004	3.51	protein kinase, cAMP dependent regulatory, type II alpha
O88712	Ctbp1	0.012	3.12	similar to CtBP1 protein; C-terminal binding protein 1
P62881	Gnb5	0.001	3.10	guanine nucleotide binding protein (G protein), beta 5
Q8BY89	Slc44a2	0.024	2.85	solute carrier family 44, member 2
Q8CGF7	Tcerg1	0.032	2.84	transcription elongation regulator 1 (CA150)
Q8BTY2	Slc4a7	0.006	2.84	solute carrier family 4, sodium bicarbonate cotransporter, member 7
Q8C0L0	Txndc13	0.005	2.82	thioredoxin-related transmembrane protein 4
P14115	Rpl27a	0.002	2.77	predicted gene 14439; predicted gene 8213; predicted gene 13981
Q99020	Hnrnpab	0.038	2.73	heterogeneous nuclear ribonucleoprotein A/B
Q8BIW1	Prune	0.031	2.71	predicted gene 5217; prune homolog (Drosophila)
Q791T5	Mtch1	0.044	2.70	mitochondrial carrier homolog 1 (C. elegans)
Q8R5J9	Arl6ip5	0.043	2.63	ADP-ribosylation factor-like 6 interacting protein 5
Q9D8E6	Rpl4	0.003	2.58	predicted gene 5835; ribosomal protein L4
P61620	Sec61a1	0.004	2.58	Sec61 alpha 1 subunit (S. cerevisiae)
Q9CR95	Necap1	0.016	2.57	NECAP endocytosis associated 1
P03893	Mtnd2	0.028	2.45	NADH-ubiquinone oxidoreductase chain 2
Q9ESW4	Agk	0.004	2.38	predicted gene 8546; acylglycerol kinase
Q8JZR6	Slc4a8	0.015	2.35	solute carrier family 4 (anion exchanger), member 8
O35609	Scamp3	0.043	2.34	secretory carrier membrane protein 3
P98086	C1qa	0.003	2.34	complement component 1, q subcomponent, alpha polypeptide
Q9D832	Dnajb4	0.041	2.23	DnaJ (Hsp40) homolog, subfamily B, member 4
P54285	Cacnb1	0.021	2.15	calcium channel, voltage-dependent, beta 3 subunit
Q8K2C9	Ptplad1	0.013	2.14	protein tyrosine phosphatase-like A domain containing 1
Q9CY27	Gpsn2	0.035	2.14	predicted gene 4948; glycoprotein, synaptic 2
Q8BVQ5	Ppme1	0.039	2.08	protein phosphatase methylesterase 1

Uniprot ID	Gene Name	p-value	Fold	Description
Q8BWQ6	UPF0505	0.041	2.06	RIKEN cDNA 9030624J02 gene
P63001	Rac1	0.029	2.02	RAS-related C3 botulinum substrate 1
P05063	Aldoc	0.041	1.95	aldolase C, fructose-bisphosphate
Q60668	Hnrnpd	0.035	1.91	heterogeneous nuclear ribonucleoprotein D
Q9JKK7	Tmod2	0.015	1.91	tropomodulin 2
Q00612	G6pdx	0.026	1.90	glucose-6-phosphate dehydrogenase X-linked
Q3UVX5	Grm5	0.048	1.88	glutamate receptor, metabotropic 5
Q9DB10	UPF0466	0.039	1.87	RIKEN cDNA 1500032L24 gene
Q07076	Anxa7	0.014	1.85	annexin A7
Q8BI08	Mal2	0.010	1.83	mal, T-cell differentiation protein 2
P14206	Rpsa	0.048	1.83	ribosomal protein SA pseudogene
Q9ERD7	Tubb3	0.043	1.80	tubulin, beta 3; tubulin, beta 3, pseudogene 1
Q3V0K9	Pls1	0.032	1.80	plastin 1 (I-isoform)
Q9JKD3	Scamp5	0.004	1.79	secretory carrier membrane protein 5
P26638	Sars	0.039	1.74	seryl-aminoacyl-tRNA synthetase
P32921	Wars	0.002	1.66	tryptophanyl-tRNA synthetase; similar to tryptophanyl-tRNA synthetase
Q8CHH9	Sept8	0.046	1.66	septin 8
Q9CPU4	Mgst3	0.025	1.65	microsomal glutathione S-transferase 3
P54775	Psmc4	0.020	1.63	proteasome (prosome, macropain) 26S subunit, ATPase, 4
P84091	Ap2m1	0.029	1.62	predicted gene 8717; adaptor protein complex AP-2, mu1
Q9CZU6	Cs	0.032	1.57	citrate synthase
Q640R3	Hepacam	0.010	1.55	hepatocyte cell adhesion molecule
Q9CPR4	Rpl17	0.019	1.55	predicted gene 8081; similar to Ribosomal protein L17;
Q8BWF0	Aldh5a1	0.025	1.54	aldhehyde dehydrogenase family 5, subfamily A1
P50396	Gdi1	0.016	1.53	guanosine diphosphate (GDP) dissociation inhibitor 1
P05201	Got1	0.046	1.47	similar to Aspartate aminotransferase
Q9D051	Pdhb	0.035	1.41	predicted gene 6123; pyruvate dehydrogenase (lipoamide) beta
P63080	Gabrb3	0.026	1.38	gamma-aminobutyric acid (GABA) A receptor, subunit beta 3
P19246	Nefh	0.021	1.38	similar to neurofilament protein; neurofilament, heavy polypeptide
P54071	Idh2	0.015	1.29	isocitrate dehydrogenase 2 (NADP+), mitochondrial
Q8BH59	Slc25a12	0.019	1.28	solute carrier family 25 (mitochondrial carrier, Aralar), member 12
Q62277	Syp	0.047	1.25	synaptophysin
Q99L43	Cds2	0.026	1.24	CDP-diacylglycerol synthase (phosphatidate cytidylyltransferase) 2
P06745	Gpi	0.010	1.12	glucose phosphate isomerase 1
Q11011	Npepps	0.023	-1.24	aminopeptidase puromycin sensitive
Q8K310	Matr3	0.032	-1.32	matrin 3; similar to Matrin 3
Q9ERS2	Ndufa13	0.034	-1.49	NADH dehydrogenase (ubiquinone) 1 alpha subcomplex, 13
O54774	Ap3d1	0.043	-1.51	adaptor-related protein complex 3, delta 1 subunit
P47802	Mtx1	0.034	-1.53	metaxin 1
P56382	Atp5e	0.038	-1.54	ATP synthase, H+ transporting, mitochondrial F1 complex, ε subunit
Q60597	Ogdh	0.041	-1.58	oxoglutarate dehydrogenase (lipoamide)
P19096	Fasn	0.022	-1.62	fatty acid synthase

Uniprot ID	Gene Name	p-value	Fold	Description
P52196	Tst	0.046	-1.62	thiosulfate sulfurtransferase, mitochondrial
Q9DCW4	Etfb	0.035	-1.65	similar to Electron transferring flavoprotein
Q9Z1B3	Plcb1	0.028	-1.67	phospholipase C, beta 1
Q9CQW1	Ykt6	0.002	-1.71	YKT6 homolog (S. Cerevisiae)
Q61316	Hspa4	0.002	-1.77	heat shock protein 4
O35683	Ndufa1	0.045	-1.80	NADH dehydrogenase (ubiquinone) 1 alpha subcomplex, 1
P54227	Stmn1	0.041	-1.81	stathmin 1; predicted gene 11223; predicted gene 6393
Q80TR1	Lphn1	0.038	-1.81	latrophilin 1
Q8BKC5	Ipo5	0.004	-1.85	hypothetical protein LOC100044315; importin 5
Q9CPP6	Ndufa5	0.035	-1.85	NADH dehydrogenase (ubiquinone) 1 alpha subcomplex, 5
Q4KMM3	Oxr1	0.019	-1.87	oxidation resistance 1
P56375	Acyp2	0.035	-1.89	acylphosphatase 2, muscle type
Q9CPW4	Arpc5	0.044	-1.90	predicted gene 16372; actin related protein 2/3 complex, subunit 5
Q8BIJ6	Iars2	0.047	-1.95	isoleucine-tRNA synthetase 2, mitochondrial
Q8BHN3	Ganab	0.017	-1.95	alpha glucosidase 2 alpha neutral subunit
Q9QUH0	Glrx	0.041	-1.97	glutaredoxin
O08788	Dctn1	0.042	-1.98	dynactin 1
P97450	Atp5j	0.046	-2.00	ATP synthase, H+ transporting, mitochondrial F0 complex, subunit F pseudogene; similar to ATP synthase coupling factor 6, mitochondrial precursor (ATPase subunit F6); ATP synthase, H+ transporting, mitochondrial F0 complex, subunit F
Q66GT5	Ptpmt1	0.022	-2.02	protein tyrosine phosphatase, mitochondrial 1
P48722	Hspa4l	0.026	-2.04	heat shock protein 4 like
A2AG50	Map7d2	0.035	-2.07	MAP7 domain containing 2
Q148V7	Kiaa1468	0.021	-2.07	RIKEN cDNA 2310035C23 gene
Q9CQ60	Pgls	0.033	-2.09	6-phosphogluconolactonase
P84089	Erh	0.049	-2.11	predicted gene 6941; enhancer of rudimentary homolog (Drosophila)
Q60902	Eps15l1	0.033	-2.12	epidermal growth factor receptor pathway substrate 15-like 1
Q8BGX2	Q8BGX2	0.025	-2.13	predicted gene 5747; RIKEN cDNA 1810026J23 gene
Q9DB70	Fundc1	0.046	-2.16	FUN14 domain containing 1
P58281	Opa1	0.026	-2.17	similar to optic atrophy 1; optic atrophy 1 homolog (human)
P70336	Rock2	0.014	-2.22	Rho-associated coiled-coil containing protein kinase 2
Q91V92	Acly	<0.001	-2.25	ATP citrate lyase
Q80UJ7	Rab3gap1	0.012	-2.27	RAB3 GTPase activating protein subunit 1
Q9JI46	Nudt3	0.012	-2.31	nudix (nucleotide diphosphate linked moiety X)-type motif 3; similar to diphosphoinositol polyphosphate phosphohydrolase
Q60865	Caprin1	0.015	-2.32	cell cycle associated protein 1
Q9D5V5	Cul5	0.042	-2.35	cullin 5
Q62446	Fkbp3	0.024	-2.40	FK506 binding protein 3
O08585	Clta	0.043	-2.40	clathrin, light polypeptide (Lca)
O54962	Banf1	0.023	-2.42	barrier to autointegration factor 1
P62627	Dynlrb1	0.030	-2.45	dynein light chain roadblock-type 1
Q0GNC1	Inf2	0.004	-2.45	subacute ozone induced inflammation
Q05920	Pc	0.006	-2.45	pyruvate carboxylase

Uniprot ID	Gene Name	p-value	Fold	Description
Q58A65	Spag9	0.022	-2.46	sperm associated antigen 9
Q8K3H0	Appl1	0.049	-2.47	adaptor protein, phosphotyrosine interaction, PH domain and leucine zipper containing 1
Q9D1C8	Vps28	0.003	-2.48	vacuolar protein sorting 28 (yeast)
Q80ZJ1	Rap2a	0.005	-2.48	RAS related protein 2a
O88653	Mapksp1	0.045	-2.49	similar to Mitogen-activated protein kinase kinase 1 interacting protein 1 (MEK binding partner 1) (Mp1); MAPK scaffold protein 1
Q61699	Hsph1	0.014	-2.49	heat shock 105kDa/110kDa protein 1
Q9EPW0	Inpp4a	0.034	-2.51	inositol polyphosphate-4-phosphatase, type I
Q9Z2H5	Epb41l1	0.028	-2.53	erythrocyte protein band 4.1-like 1
P97493	Txn2	0.046	-2.55	thioredoxin 2
Q8BWR2	Trp26	0.040	-2.55	RIKEN cDNA 1110049F12 gene
Q9CQI3	Gmfb	0.017	-2.57	glia maturation factor, beta
P61971	Nutf2	0.022	-2.58	similar to Chain A, D92n,D94n Double Point Mutant Of Human Nuclear Transport Factor 2 (Ntf2); nuclear transport factor 2;
P84086	Cplx2	0.015	-2.58	complexin 2
Q8BGQ7	Aars	0.026	-2.63	alanyl-tRNA synthetase
Q8VCT3	Rnpep	0.020	-2.65	arginyl aminopeptidase (aminopeptidase B)
Q80Y14	Glrx5	0.034	-2.68	glutaredoxin 5 homolog (S. cerevisiae)
Q9CQ85	Timm22	0.017	-2.69	translocase of inner mitochondrial membrane 22 homolog (yeast)
Q811D0	Dlg1	0.044	-2.69	discs, large homolog 1 (Drosophila); similar to Discs, large homolog 1 (Drosophila)
Q9CQ69	Uqcrq	0.019	-2.70	ubiquinol-cytochrome c reductase, complex III subunit VII
Q91VR8	Brk1	0.030	-2.70	RIKEN cDNA 6720456B07 gene
O35127	Grcc10	0.048	-2.72	gene rich cluster, C10 gene
O88851	Rbbp9	0.024	-2.76	retinoblastoma binding protein 9; similar to Retinoblastoma-binding protein 9 (RBBP-9) (B5T overexpressed gene protein) (Bog protein)
Q8BGS2	Bola2	0.024	-2.78	bolA-like 2 (E. coli)
P27546	Map4	0.018	-2.80	microtubule-associated protein 4
Q9EQ80	Nif3l1	0.031	-2.81	Ngg1 interacting factor 3-like 1 (S. pombe)
Q61330	Cntn2	0.020	-2.82	contactin 2
Q9WVL0	Gstz1	0.004	-2.89	glutathione transferase zeta 1 (maleylacetoacetate isomerase)
Q9D0R2	Tars	0.030	-2.89	threonyl-tRNA synthetase
Q9JKR6	Hyou1	0.044	-2.96	hypoxia up-regulated 1
Q9CZD3	Gars	0.009	-3.06	glycyl-tRNA synthetase
Q9CQX8	Mrps36	0.028	-3.13	predicted gene 10078; predicted gene 3544; similar to mitochondrial ribosomal protein S36; mitochondrial ribosomal protein S36
Q8VD37	Sgip1	0.035	-3.27	SH3-domain GRB2-like (endophilin) interacting protein 1
Q8BU30	Iars	0.046	-3.28	isoleucine-tRNA synthetase
P23116	Eif3a	0.013	-3.38	eukaryotic translation initiation factor 3, subunit A
Q8VBV7	Cops8	0.031	-3.44	COP9 (constitutive photomorphogenic) homolog, subunit 8
Q61301	Ctnna2	0.048	-3.44	catenin (cadherin associated protein), alpha 2
Q9D7X8	Ggct	0.046	-3.46	gamma-glutamyl cyclotransferase
Q80X50	Ubap2l	0.049	-3.49	ubiquitin associated protein 2-like
P28740	Kif2a	0.011	-3.52	kinesin family member 2A
P21619	Lmnb2	0.042	-3.60	lamin B2

Uniprot ID	Gene Name	p-value	Fold	Description
P28271	Aco1	0.020	-3.61	aconitase 1
P60469	Ppfia3	0.021	-3.65	protein tyrosine phosphatase, receptor type, f polypeptide (PTPRF), interacting protein (liprin), alpha 3
Q8BRT1	Clasp2	0.016	-3.67	CLIP associating protein 2
Q9QYB5	Add3	0.026	-3.72	adducin 3 (gamma)
Q80UG2	Plxna4	0.004	-3.76	plexin A4
Q9QWI6	P140	0.017	-3.89	P140 gene
O70161	Pip5k1c	0.016	-3.93	phosphatidylinositol-4-phosphate 5-kinase, type 1 gamma
Q8CGY8	Ogt	0.014	-4.02	O-linked N-acetylglucosamine (GlcNAc) transferase (UDP-N-acetylglucosamine:polypeptide-N-acetylglucosaminyl transferase)
P61458	Pcbd1	0.035	-4.15	pterin 4 alpha carbinolamine dehydratase/dimerization cofactor of hepatocyte nuclear factor 1 alpha (TCF1) 1
Q9JMH9	Myo18a	0.022	-4.30	myosin XVIIIA
Q3U0V1	Khsrp	0.002	-4.32	KH-type splicing regulatory protein
P35123	Usp11	<0.001	-4.40	ubiquitin specific peptidase 4 (proto-oncogene)
Q64737	Gart	0.011	-4.57	phosphoribosylglycinamide formyltransferase
Q3UPL0	Sec31a	0.008	-4.66	Sec31 homolog A (S. cerevisiae)
Q9DBR7	Ppp1r12a	0.009	-4.79	protein phosphatase 1, regulatory (inhibitor) subunit 12A
Q9EQQ9	Mgea5	0.011	-5.00	meningioma expressed antigen 5 (hyaluronidase)
Q9DB27	Mcts1	0.034	-5.03	malignant T cell amplified sequence 1
Q91YE6	Ipo9	0.029	-5.50	importin 9
Q9QXL2	Kif21a	0.022	-5.61	kinesin family member 21A
Q4ACU6	Shank3	0.011	-5.85	SH3/ankyrin domain gene 3
Q9Z130	Hnrpdl	0.035	-6.04	heterogeneous nuclear ribonucleoprotein D-like
Q9CXW3	Cacybp	0.018	-6.74	calcyclin binding protein
Q6P9K8	Caskin1	0.043	-6.95	CASK interacting protein 1
Q7TMB8	Cyfip1	0.001	-7.32	cytoplasmic FMR1 interacting protein 1
Q80U40	Rimbp2	0.015	-7.67	RIMS binding protein 2
P02468	Lamc1	0.010	-10.86	laminin, gamma 1
Q3UHD9	Agap2	<0.001	-11.45	ArfGAP with GTPase domain, ankyrin repeat and PH domain 2
P08556	Nras		↓	similar to neuroblastoma ras oncogene; neuroblastoma ras oncogene
P36536	Sar1a		↓	SAR1 gene homolog A (S. cerevisiae)
P39054	Dnm2		↓	dynamin 2
P58059	Mrps21		↓	mitochondrial ribosomal protein S21; predicted gene 6686; predicted gene 6181
P59708	Sf3b14		↓	RIKEN cDNA 0610009D07 gene
P61148	Fgf1		↓	fibroblast growth factor 1
P98203	Arvcf		↓	armadillo repeat gene deleted in velo-cardio-facial syndrome
Q03173	Enah		↓	enabled homolog (Drosophila)
Q05A62	Dnal1		↓	dynein, axonemal, light chain 1
Q3TDD9	Klraq1		↓	KLRAQ motif containing 1
Q3TES0	Iqsec3		↓	IQ motif and Sec7 domain 3
Q3U487	Hectd3		↓	HECT domain containing 3
Q3UH68	Limch1		↓	LIM and calponin homology domains 1

Uniprot ID	Gene Name	p-value	Fold	Description
Q3UU96	Cdc42bpa		↓	CDC42 binding protein kinase alpha
Q5F2E8	Taok1		↓	TAO kinase 1
Q5SSM3	Rich2		↓	expressed sequence AU040829
Q5SXY1	Specc1		↓	cytospin B
Q5XJV6	Lmtk3		↓	lemur tyrosine kinase 3
Q64152	Btf3		↓	predicted gene 9308; basic transcription factor 3;
Q69ZW3	Ehbp1		↓	EH domain binding protein 1
Q6A065	Cep170		↓	centrosomal protein 170
Q6NVE8	Wdr44		↓	WD repeat domain 44
Q6PAR5	Gapvd1		↓	GTPase activating protein and VPS9 domains 1
Q6PDI5	Ecm29		↓	expressed sequence AI314180
Q6PFD5	Dlgap3		↓	discs, large (Drosophila) homolog-associated protein 3
Q6Y7W8	Gigyf2		↓	GRB10 interacting GYF protein 2
Q7SIG6	Asap2		↓	development and differentiation enhancing factor 2
Q7TSC1	Bat2		↓	HLA-B associated transcript 2
Q80U49	Kiaa0284		↓	expressed sequence AW555464
Q810B6	Ankfy1		↓	ankyrin repeat and FYVE domain containing 1
Q8BGR6	Arl15		↓	ADP-ribosylation factor-like 15
Q8BLY2	Tarsl2		↓	threonyl-tRNA synthetase-like 2
Q8BMI3	Gga3		↓	golgi associated, gamma adaptin ear containing, ARF binding protein 3
Q8BPM0	Daam1		↓	dishevelled associated activator of morphogenesis 1
Q8BY87	Usp47		↓	ubiquitin specific peptidase 47
Q8C1B1	Camsap1l1		↓	calmodulin regulated spectrin-associated protein 1-like 1
Q8CC88	Kiaa0564		↓	RIKEN cDNA 1300010F03 gene
Q8CCN5	Bcas3		↓	breast carcinoma amplified sequence 3
Q8CDG3	Vcpip1		↓	valosin containing protein (p97)/p47 complex interacting protein 1
Q8K394	Plcl2		↓	phospholipase C-like 2
Q8QZZ7	Tprkb		↓	Tp53rk binding protein
Q8R4H2	Arhgef12		↓	similar to SP140 nuclear body protein (predicted); Rho guanine nucleotide exchange factor (GEF) 12
Q91WV0	Dr1		↓	down-regulator of transcription 1
Q923D5	Wbp11		↓	WW domain binding protein 11
Q9CPW2	Fdx1l		↓	ferredoxin 1-like
Q9CQV7	Dnajc19		↓	DnaJ (Hsp40) homolog, subfamily C, member 19
Q9CQZ1	Hsbp1		↓	heat shock factor binding protein 1
Q9D0L7	Armc10		↓	predicted gene 9209; armadillo repeat containing 10
Q9D1L0	Chchd2		↓	coiled-coil-helix-coiled-coil-helix domain containing 2; predicted gene 13202; similar to coiled-coil-helix-coiled-coil-helix domain containing 2; predicted gene 12350
Q9D8S9	Bola1		↓	bolA-like 1 (E. coli)
Q9D8T7	Slirp		↓	RIKEN cDNA 1810035L17 gene
Q9ERG2	Strn3		↓	striatin, calmodulin binding protein 3
Q9ERU9	Ranbp2		↓	RAN binding protein 2
Q9JKL4	Ndufaf3		↓	NADH dehydrogenase (ubiquinone) 1 alpha subcomplex, assembly factor 3

Uniprot ID	Gene Name	p-value	Fold	Description
Q9JL26	Fmnl1		↓	formin-like 1
Q9QWY8	Asap1		↓	similar to Development and differentiation enhancing; ArfGAP with SH# domain, ankyrin repeat and PH domain1
Q9R1Z7	Pts		↓	6-pyruvoyl-tetrahydropterin synthase
Q9Z2I2	Fkbp1b		↓	FK506 binding protein 1b
Q9Z2V5	Hdac6		↓	histone deacetylase 6

Table 2

Functional categories of terms from the proteomic and transcriptomic significant changes

Functional categories are ranked by the % of the total proteomic terms.

	Proteomic			Transcriptomic		
Functional category	**Terms**	**% of terms**	**Proteins**	**terms**	**% of terms**	**Genes**
cytoskeleton	62	8.4	66	3	1.3	3
neuron	59	8.0	41	3	1.3	4
transcription	48	6.5	47	14	6.1	4
mitochondria	47	6.3	80	4	1.7	8
signaling	37	5.0	47	5	2.2	5
ion transport/channels	35	4.7	34	7	3.0	8
nucleus	30	4.0	69	1	0.4	3
vesicle	30	4.0	37	24	10.4	14
metabolism	28	3.8	20	8	3.5	9
transport	25	3.4	51	1	0.4	7
development	13	1.8	12	4	1.7	5
extracellular matrix/adhesion	12	1.6	15	10	4.3	28
apoptosis	12	1.6	7	5	2.2	5
immune	8	1.1	12	66	28.7	45
protein modification	11	1.5	25			
neural disease	10	1.3	13			
ubiquitin	10	1.3	12			
cell cycle	6	0.8	8			
unassigned terms	259	34.9		75	32.6	

Table 3
Significant mitochondrial proteomic changes found in the MitoCarta database

uniprot #	Gene	p-value	fold	Description
Q924L1	Letmd1		↑	LETM1 domain containing 1
Q791T5	Mtch1	0.044	2.70	Mitochondrial carrier homolog 1
P26638	Sars	0.039	1.74	Seryl-tRNA synthetase, cytoplasmic
Q9CZU6	Cs	0.033	1.57	Citrate synthase, mitochondrial
Q8BWF0	Aldh5a1	0.025	1.54	Succinate-semialdehyde dehydrogenase, mitochondrial
Q9D051	Pdhb	0.035	1.41	Pyruvate dehydrogenase E1 component subunit beta, mitochondrial
P54071	Idh2	0.016	1.29	Isocitrate dehydrogenase [NADP], mitochondrial
Q8BH59	Slc25a12	0.019	1.28	Calcium-binding mitochondrial carrier protein Aralar1
Q9ERS2	Ndufa13	0.034	-1.49	NADH dehydrogenase [ubiquinone] 1 alpha subcomplex subunit 13
P47802	Mtx1	0.034	-1.53	Metaxin-1
P56382	Atp5e	0.038	-1.54	ATP synthase subunit epsilon, mitochondrial
Q60597	Ogdh	0.040	-1.58	2-oxoglutarate dehydrogenase E1 component, mitochondrial
P19096	Fasn	0.022	-1.62	Fatty acid synthase
P52196	Tst	0.046	-1.62	Thiosulfate sulfurtransferase
Q9DCW4	Etfb	0.036	-1.65	Electron transfer flavoprotein subunit beta
O35683	Ndufa1	0.045	-1.80	NADH dehydrogenase [ubiquinone] 1 alpha subcomplex subunit 1
Q9CPP6	Ndufa5	0.035	-1.85	NADH dehydrogenase [ubiquinone] 1 alpha subcomplex subunit 5
Q4KMM3	Oxr1	0.019	-1.87	Oxidation resistance protein 1
P56375	Acyp2	0.035	-1.89	Acylphosphatase-2
Q8BIJ6	Iars2	0.047	-1.95	Isoleucyl-tRNA synthetase, mitochondrial
Q9QUH0	Glrx	0.041	-1.97	Glutaredoxin-1
P97450	Atp5j	0.046	-2.00	ATP synthase-coupling factor 6, mitochondrial
Q66GT5	Ptpmt1	0.022	-2.02	Protein-tyrosine phosphatase mitochondrial 1
P58281	Opa1	0.027	-2.17	Dynamin-like 120 kDa protein, mitochondrial
Q91V92	Acly	<0.0003	-2.25	ATP-citrate synthase
P97493	Txn2	0.045	-2.55	Thioredoxin, mitochondrial
Q80Y14	Glrx5	0.034	-2.68	Glutaredoxin-related protein 5
Q9CQ85	Timm22	0.017	-2.69	Mitochondrial import inner membrane translocase subunit Tim22
Q9CQ69	Uqcrq	0.019	-2.70	Cytochrome b-c1 complex subunit 8
Q9EQ80	Nif3l1	0.031	-2.81	NIF3-like protein 1
Q9CZD3	Gars	0.009	-3.06	Glycyl-tRNA synthetase
Q9CQX8	Mrps36	0.028	-3.13	28S ribosomal protein S36, mitochondrial
P28271	Aco1	0.020	-3.61	Cytoplasmic aconitate hydratase
Q9D8S9	Bola1		↓	BolA-like protein 1
Q9R1Z7	Pts		↓	6-pyruvoyl tetrahydrobiopterin synthase
P58059	Mrps21		↓	28S ribosomal protein S21, mitochondrial
Q9D1L0	Chchd2		↓	Coiled-coil-helix-domain-containing protein 2, mitochondrial
Q9CQV7	Dnajc19		↓	Mitochondrial import inner membrane translocase subunit TIM14

Table 4

Mitochondrial proteins detected and changed by Palmfeld functional subcategories [28]

Protein category	proteins	detected	changed	% detected	% significant
Citric acid cycle	30	25	6	83%	24%
Mitochondrial morphology	12	6	1	50%	17%
Mitochondrial translation	99	44	7	44%	16%
Antioxidant systems	33	17	2	52%	12%
Respiratory chain	82	58	5	71%	9%
Amino acid metabolism	64	35	3	55%	9%
Fatty acid metabolism	21	18	1	86%	6%
Protein quality control systems	16	12	0	75%	0%
Apoptosis	7	3	0	43%	0%
Known disease association (OMIM database)	36	31	5	86%	16%

Mol Genet Metab. Author manuscript; available in PMC 2017 May 01.

Table 5

Proteomic changes associated with energy generating categories

A. G lycolysis				**C. Respiratory chain**					
Gene	**p-value**	**fold**		**Gene**	**p-value**	**fold**	**Gene**	**p-value**	**fold**
Increases				**Complex 1**			**Complex 4**		
Aldoc	**0.040**	**1.95**	1	***Increases***			***Increases***		
Aldoa	0.207	1.47		Ndufv1	0.080	1.43	Cox6a1	0.877	1.06
Pgk1	0.204	1.36		Ndufs2	0.311	1.29	***Decreases***		
Pkm2	0.168	1.32		Ndufa8	0.069	1.20	Cox4i1	0.950	-1.01
Pgam1	0.389	1.31		Ndufa9	0.100	1.18	Cox6c	0.859	-1.08
Eno1	0.324	1.21		Ndufb11	0.544	1.18	Cox5b	0.530	-1.24
Eno3	0.349	1.2		Ndufs3	0.430	1.15	Cox6b1	0.271	-1.26
Eno2	0.296	1.2		Ndufs8	0.666	1.08	Cox5a	0.079	-1.26
Pfkl	0.567	1.12		***Decreases***			Cox7a2	0.536	-1.29
Gpi	**0.010**	**1.12**		Ndufs1	0.735	-1.04	Cox7a2l	0.275	-1.95
Tpi1	0.807	1.08		Ndufa6	0.791	-1.06	Cox7a1	0.168	-2.11
Gapdh	0.661	1.07		Ndufa10	0.671	-1.09	**ATP synthase**		
Pfkm	0.918	1.02		Ndufb5	0.506	-1.11	***Increases***		
Decreases				Ndufa2	0.078	-1.14	Atp5a1	0.100	1.40
Pfkp	0.696	-1.04		Ndufb10	0.708	-1.17	Atp5b	0.089	1.33
Hk1	0.241	-1.14		Ndufa7	0.811	-1.18	Atp5o	0.188	1.07
				Ndufs6	0.703	-1.19	Atp5j2	0.969	1.01
				Ndufa12	0.464	-1.21	***Decreases***		
				Ndufa4	0.052	-1.23	Atp5h	0.869	-1.03
				Ndufb6	0.600	-1.24	Atp5c1	0.852	-1.06
B. Citric acid cycle				Ndufb7	0.361	-1.25	Atp5f1	0.447	-1.11
Gene	**p-value**	**fold**		Ndufs5	0.358	-1.27	Atp5l	0.213	-1.16
Increases				Ndufs7	0.385	-1.30	Atp5d	0.489	-1.35
Dlst	0.063	2.11		Ndufc2	0.286	-1.31	**Atp5e**	**0.038**	**-1.54**
Clybl	0.278	1.7		Ndufb3	0.434	-1.39	Atp5i	0.086	-1.72

A. G lycolysis				C. Respiratory chain							
Gene	**p-value**	**fold**		**Gene**	**p-value**	**fold**		**Gene**	**p-value**	**fold**
Increases				**Complex 1**				**Complex 4**		
Cs	**0.033**	**1.57**		Ndufb8	0.148	-1.43		**Atp5j**	**0.046**	**-2.00**
Pdha1	0.090	1.57		Ndufv2	0.327	-1.48		**Atp5s**		↓
Fh	0.201	1.53		**Ndufa13**	**0.034**	**-1.49**		**Other**		
Dld	0.075	1.46		Ndufb9	0.081	-1.60		***Increases***		
Idh3a	0.130	1.43		Ndufv3	0.477	-1.62		Etfdh	0.386	1.91
Mdh2	0.126	1.43		**Ndufa1**	**0.045**	**-1.80**		Etfa	0.597	1.26
Pdhb	**0.035**	**1.41**		Ndufs4	0.287	-1.81		Cyb5b	0.686	1.14
Dlat	0.092	1.39		**Ndufa5**	**0.035**	**-1.85**		***Decreases***		
Sucla2	0.425	1.31		Ndufb2	0.272	-1.89		Cyc1	0.776	-1.09
Sdhb	0.449	1.3	2	Ndufab1	0.089	-2.44		**Etfb**	**0.036**	**-1.65**
Idh2	**0.016**	**1.29**		**Ndufa3**		↓		Txnl1	0.360	-1.94
Sdhc	0.386	1.26	2	**Complex 3**				**Fdx1**		↓
Suclg1	0.629	1.25		***Increases***				**Fdx1l**		↓
Pdk1	0.731	1.2		Uqcrc1	0.066	1.81				
Sdha	0.557	1.16	2	Uqcrc2	0.145	1.53				
Sdhd	0.790	1.09	2	***Decreases***						
Idh3g	0.819	1.07		Uqcrfs1	0.902	-1.02				
Aco2	0.878	1.03		Uqcr10	0.155	-1.30				
Decreases				Uqcrh	0.085	-1.88				
Ogdh	**0.040**	**-1.58**		**Uqcrq**	**0.019**	**-2.70**				

Changes in bold detected at p<0.05 or exclusively in one group; 2 Complex 2 (Sdh) proteins included with the citric acid cycle proteins

Table 6

Significant cytoskeletal protein changes ($p<0.05$ or exclusively in one group).

Uniprot #	Gene Name	p-value	fold	Description
P10922	H1f0		↑	Histone H1.0
Q9EPR4	Slc23a2		↑	Solute carrier family 23 member 2
Q8BTY2	Slc4a7	0.006	2.84	Sodium bicarbonate cotransporter 3
P14115	Rpl27a	0.002	2.77	60S ribosomal protein L27a
Q8BIW1	Prune	0.031	2.71	Protein prune homolog
Q8R5J9	Arl6ip5	0.043	2.63	PRA1 family protein 3
Q9D8E6	Rpl4	0.003	2.58	60S ribosomal protein L4
P54285	Cacnb1	0.021	2.15	Voltage-dependent L-type calcium channel subunit beta-1
P63001	Rac1	0.029	2.02	Ras-related C3 botulinum toxin substrate 1
Q60668	Hnrnpd	0.036	1.91	Heterogeneous nuclear ribonucleoprotein D0
Q9JKK7	Tmod2	0.015	1.91	Tropomodulin-2
P14206	Rpsa	0.048	1.83	40S ribosomal protein SA
Q9ERD7	Tubb3	0.043	1.80	Tubulin beta-3 chain
Q3V0K9	Pls1	0.032	1.80	Plastin-1
Q8CHH9	sept8	0.046	1.66	Septin-8
Q9CPR4	Rpl17	0.020	1.55	60S ribosomal protein L17
P19246	Nefh	0.021	1.38	Neurofilament heavy polypeptide
Q9ERS2	Ndufa13	0.034	-1.49	NADH dehydrogenase [ubiquinone] 1 alpha subcomplex subunit 13
P54227	Stmn1	0.040	-1.81	Stathmin
Q4KMM3	Oxr1	0.019	-1.87	Oxidation resistance protein 1
Q9CPW4	Arpc5	0.044	-1.90	Actin-related protein 2/3 complex subunit 5
O08788	Dctn1	0.042	-1.98	Dynactin subunit 1
P70336	Rock2	0.014	-2.22	Rho-associated protein kinase 2
O54962	Banf1	0.023	-2.42	Barrier-to-autointegration factor
Q0GNC1	Inf2	0.004	-2.45	Inverted formin-2
P62627	Dynlrb1	0.030	-2.45	Dynein light chain roadblock-type 1
Q58A65	Spag9	0.022	-2.46	C-jun-amino-terminal kinase-interacting protein 4
Q9Z2H5	Epb41l1	0.027	-2.53	Band 4.1-like protein 1
Q9CQI3	Gmfb	0.017	-2.57	Glia maturation factor beta
Q811D0	Dlg1	0.044	-2.69	Disks large homolog 1
Q91VR8	Brick1	0.030	-2.70	Probable protein BRICK1
P27546	Map4	0.018	-2.80	Microtubule-associated protein 4
Q9CQX8	Mrps36	0.028	-3.13	28S ribosomal protein S36, mitochondrial
P23116	Eif3a	0.012	-3.38	Eukaryotic translation initiation factor 3 subunit A
Q61301	Ctnna2	0.048	-3.44	Catenin alpha-2
P28740	Kif2a	0.011	-3.52	Kinesin-like protein KIF2A
P21619	Lmnb2	0.041	-3.60	Lamin-B2
Q8BRT1	Clasp2	0.016	-3.67	CLIP-associating protein 2
Q9QYB5	Add3	0.026	-3.72	Gamma-adducin

Uniprot #	Gene Name	p-value	fold	Description
Q9QWI6	P140	0.017	-3.89	p130Cas-associated protein
O70161	Pip5k1c	0.016	-3.93	Phosphatidylinositol-4-phosphate 5-kinase type-1 gamma
Q9JMH9	Myo18a	0.023	-4.30	Myosin-XVIIIa
Q9DBR7	Ppp1r12a	0.009	-4.79	Protein phosphatase 1 regulatory subunit 12A
Q9QXL2	Kif21a	0.022	-5.61	Kinesin-like protein KIF21A
Q4ACU6	Shank3	0.012	-5.85	SH3 and multiple ankyrin repeat domains protein 3
Q6P9K8	Caskin1	0.042	-6.95	Caskin-1
Q7TMB8	Cyfip1	0.001	-7.32	Cytoplasmic FMR1-interacting protein 1
Q80U40	Rimbp2	0.015	-7.67	RIMS-binding protein 2
Q3UHD9	Agap2	<0.000003	-11.45	Arf-GAP, GTPase, ANK repeat and PH domain-containing protein 2
P08556	Nras		↓	GTPase NRas
Q9QWY8	Asap1		↓	Arf-GAP with SH3 domain, ANK repeat and PH domain-containing protein 1
P58059	Mrps21		↓	28S ribosomal protein S21, mitochondrial
Q03173	Enah		↓	Protein enabled homolog
Q6PFD5	Dlgap3		↓	Disks large-associated protein 3
Q923D5	Wbp11		↓	WW domain-binding protein 11
Q80U49	Kiaa0284		↓	Protein KIAA0284
Q6A065	Cep170		↓	Centrosomal protein of 170 kDa
Q6PDI5	Ecm29		↓	Proteasome-associated protein ECM29 homolog
Q8C1B1	Camsap1l1		↓	Calmodulin-regulated spectrin-associated protein 1-like protein 1
P39054	Dnm2		↓	Dynamin-2
Q3UH68	Limch1		↓	LIM and calponin homology domains-containing protein 1
Q3UU96	Cdc42bpa		↓	Serine/threonine-protein kinase MRCK alpha
Q7SIG6	Asap2		↓	Arf-GAP with SH3 domain, ANK repeat and PH domain-containing protein 2
Q810B6	Ankfy1		↓	Ankyrin repeat and FYVE domain-containing protein 1
Q8BPM0	Daam1		↓	Disheveled-associated activator of morphogenesis 1
Q9JL26	Fmnl1		↓	Formin-like protein 1

Table 7

Significant transcriptomic changes in the Bl6 hippocampus (q< 0.05 and fold >1.5).

Probeset ID	Gene Symbol	Gene Title	Fold	q-value
1420699_at	Clec7a	C-type lectin domain family 7, member a	11.2	<0.01
1419202_at	Cst7	cystatin F (leukocystatin)	10.6	<0.01
1448303_at	Gpnmb	glycoprotein (transmembrane) nmb	9.8	<0.01
1423547_at	Lyz2	lysozyme 2	7.4	<0.01
1436996_x_at	Lyz1	lysozyme 1	7.0	<0.01
1439426_x_at	Lyz1	lysozyme 1	7.0	<0.01
1426509_s_at	Gfap	glial fibrillary acidic protein	5.9	<0.01
1418021_at	C4b	complement component 4B (Childo blood group)	5.7	<0.01
1426808_at	Lgals3	lectin, galactose binding, soluble 3	5.5	<0.01
1420394_s_at	Gp49a /// Lilrb4	glycoprotein 49 A /// leukocyte immunoglobulin-like receptor, subfamily B, member 4	4.9	<0.01
1426508_at	Gfap	glial fibrillary acidic protein	4.9	<0.01
1435477_s_at	Fcgr2b	Fc receptor, IgG, low affinity IIb	4.3	<0.01
1427076_at	Mpeg1	macrophage expressed gene 1	4.2	<0.01
1424754_at	Ms4a7	membrane-spanning 4-domains, subfamily A, member 7	4.1	<0.01
1449164_at	Cd68	CD68 antigen	4.0	<0.01
1419004_s_at	Bcl2a1a /// Bcl2a1b /// Bcl2a1d	B-cell leukemia/lymphoma 2 related protein A1a /// B-cell leukemia/ lymphoma 2 related p	4.0	<0.01
1418808_at	Rdh5	retinol dehydrogenase 5	4.0	0.027
1419100_at	Serpina3n	serine (or cysteine) peptidase inhibitor, clade A, member 3N	3.8	0.014
1427301_at	Cd48	CD48 antigen	3.6	<0.01
1419561_at	Ccl3	chemokine (C-C motif) ligand 3	3.4	<0.01
1437540_at	Mcoln3	mucolipin 3	3.2	<0.01
1448021_at	Fam46c	family with sequence similarity 46, member C	3.0	<0.01
1422875_at	Cd84	CD84 antigen	2.9	<0.01
1421792_s_at	Trem2	triggering receptor expressed on myeloid cells 2	2.9	<0.01
1452352_at	Ctla2b	cytotoxic T lymphocyte-associated protein 2 beta	2.8	0.014
1451941_a_at	Fcgr2b	Fc receptor, IgG, low affinity IIb	2.7	<0.01
1428114_at	Slc14a1	solute carrier family 14 (urea transporter), member 1	2.7	0.041
1427221_at	Slc6a20a	solute carrier family 6 (neurotransmitter transporter), member 20A	2.7	0.014
1449401_at	C1qc	complement component 1, q subcomponent, C chain	2.7	<0.01
1455332_x_at	Fcgr2b	Fc receptor, IgG, low affinity IIb	2.6	<0.01
1419598_at	Ms4a6d	membrane-spanning 4-domains, subfamily A, member 6D	2.6	<0.01
1454268_a_at	Cyba	cytochrome b-245, alpha polypeptide	2.6	0.041
1419298_at	Pon3	paraoxonase 3	2.5	0.041
1448710_at	Cxcr4	chemokine (C-X-C motif) receptor 4	2.5	<0.01
1418028_at	Dct	dopachrome tautomerase	2.4	0.041
1419482_at	C3ar1	complement component 3a receptor 1	2.4	<0.01
1437726_x_at	C1qb	complement component 1, q subcomponent, beta polypeptide	2.4	0.014
1419599_s_at	Ms4a6d	membrane-spanning 4-domains, subfamily A, member 6D	2.3	<0.01

Probeset ID	Gene Symbol	Gene Title	Fold	q-value
1416612_at	Cyp1b1	cytochrome P450, family 1, subfamily b, polypeptide 1	2.3	<0.01
1452014_a_at	Igf1	insulin-like growth factor 1	2.3	<0.01
1434366_x_at	C1qb	complement component 1, q subcomponent, beta polypeptide	2.2	0.027
1424067_at	Icam1	intercellular adhesion molecule 1	2.2	0.014
1451161_a_at	Emr1	EGF-like module containing, mucin-like, hormone receptor-like sequence 1	2.2	<0.01
1449156_at	Ly9	lymphocyte antigen 9	2.2	<0.01
1448380_at	Lgals3bp	lectin, galactoside-binding, soluble, 3 binding protein	2.2	<0.01
1419483_at	C3ar1	complement component 3a receptor 1	2.1	<0.01
1419128_at	Itgax	integrin alpha X	2.0	<0.01
1422660_at	Rbm3	RNA binding motif protein 3	2.0	0.027
1421223_a_at	Anxa4	annexin A4	2.0	<0.01
1448148_at	Grn	granulin	2.0	0.014
1420361_at	Slc11a1	solute carrier family 11 (proton-coupled divalent metal ion transporters), member 1	1.9	<0.01
1417963_at	Pltp	phospholipid transfer protein	1.9	0.014
1451784_x_at	H2-D1	histocompatibility 2, D region locus 1	1.9	0.038
1425545_x_at	H2-D1	histocompatibility 2, D region locus 1	1.9	0.014
1451683_x_at	H2-D1	histocompatibility 2, D region locus 1	1.9	0.041
1419315_at	Slamf9	SLAM family member 9	1.9	0.014
1419132_at	Tlr2	toll-like receptor 2	1.8	<0.01
1417870_x_at	Ctsz	cathepsin Z	1.8	<0.01
1448640_at	Slc14a1	solute carrier family 14 (urea transporter), member 1	1.8	0.032
1417868_a_at	Ctsz	cathepsin Z	1.8	<0.01
1448591_at	Ctss	cathepsin S	1.8	0.014
1448891_at	Fcrls	Fc receptor-like S, scavenger receptor	1.8	<0.01
1435903_at	Cd300a	CD300A antigen	1.7	0.027
1419455_at	Il10rb	interleukin 10 receptor, beta	1.7	<0.01
1416527_at	Rab32	RAB32, member RAS oncogene family	1.7	0.014
1426025_s_at	Laptm5	lysosomal-associated protein transmembrane 5	1.7	0.014
1425025_at	Tmem106a	transmembrane protein 106A	1.7	0.014
1418826_at	Ms4a6b	membrane-spanning 4-domains, subfamily A, member 6B	1.7	<0.01
1418910_at	Bmp7	bone morphogenetic protein 7	1.7	<0.01
1428018_a_at	AF251705	cDNA sequence AF251705	1.7	0.014
1460248_at	Cpxm2	carboxypeptidase X 2 (M14 family)	1.6	0.014
1436890_at	Uap1l1	UDP-N-acteylglucosamine pyrophosphorylase 1-like 1	1.6	0.014
1456567_x_at	Grn	granulin	1.6	<0.01
1438910_a_at	Stom	stomatin	1.5	0.014
1418825_at	Irgm1	immunity-related GTPase family M member 1	1.5	0.014
1449195_s_at	Cxcl16	chemokine (C-X-C motif) ligand 16	1.5	0.014
1416340_a_at	Man2b1	mannosidase 2, alpha B1	1.5	0.014
1421812_at	Tapbp	TAP binding protein	1.5	0.027
1448606_at	Lpar1	lysophosphatidic acid receptor 1	-2.1	<0.01

Probeset ID	Gene Symbol	Gene Title	Fold	q-value
1455965_at	Adamts4	a disintegrin-like and metallopeptidase (reprolysin type) with thrombospondin type 1 mo	-2.1	0.041
1419064_a_at	Ugt8a	UDP galactosyltransferase 8A	-2.6	0.041

Table 8
Shared transcriptomic and proteomic terms grouped by assigned functional category

Immune	Mitochondria
GO:0001775-cell activation	GO:0005739-mitochondrion
GO:0002252-immune effector process	GO:0031090-organelle membrane
GO:0002443-leukocyte mediated immunity	GO:0055114-oxidation reduction
GO:0002684-positive regulation of immune system process	**Development**
GO:0006955-immune response	GO:0035239-tube morphogenesis
GO:0007186-G-protein coupled receptor protein signaling pathway	GO:0035295-tube development
GO:0010033-response to organic substance	nucleus
GO:0016192-vesicle-mediated transport	GO:0000166-nucleotide binding
GO:0045321-leukocyte activation	**Transcription**
IPR013783:Immunoglobulin-like fold	GO:0045449-regulation of transcription
transducer	**Transport**
Vesicle	transport
cytoplasmic vesicle	**Not assigned**
GO:0006897-endocytosis	acetylation
GO:0010324-membrane invagination	alternative splicing
GO:0016023-cytoplasmic membrane-bounded vesicle	cell membrane
GO:0016044-membrane organization	cytoplasm
GO:0031410-cytoplasmic vesicle	disulfide bond
GO:0031982-vesicle	glycoprotein
GO:0031988-membrane-bounded vesicle	glycosylation site:N-linked (GlcNAc…)
GO:0051130-positive regulation of cellular component organization	GO:0000267-cell fraction
mmu04142:Lysosome	GO:0005506-iron ion binding
Extracellular matrix/Adhesion	GO:0005615-extracellular space
cell adhesion	GO:0005624-membrane fraction
GO:0005576-extracellular region	GO:0005626-insoluble fraction
GO:0007155-cell adhesion	GO:0005783-endoplasmic reticulum
GO:0022610-biological adhesion	GO:0005886-plasma membrane
GO:0044421-extracellular region part	GO:0006355-regulation of transcription, DNA-dependent
Secreted	GO:0007166-cell surface receptor linked signal transduction
Apoptosis	GO:0007242-intracellular signaling cascade
GO:0008219-cell death	GO:0008270-zinc ion binding
GO:0010941-regulation of cell death	GO:0008283-cell proliferation
GO:0016265-death	GO:0010604-positive regulation of macromolecule metabolic process
GO:0042981-regulation of apoptosis	GO:0016021-integral to membrane
GO:0043067-regulation of programmed cell death	GO:0031224-intrinsic to membrane
Metabolism	GO:0042127-regulation of cell proliferation

Immune	Mitochondria
GO:0006508-proteolysis	GO:0042470-melanosome
GO:0008233-peptidase activity	GO:0043167-ion binding
GO:0008234-cysteine-type peptidase activity	GO:0043169-cation binding
GO:0070011-peptidase activity, acting on L-amino acid peptides	GO:0044459-plasma membrane part
Protease	GO:0046872-metal ion binding
Signaling	GO:0046914-transition metal ion binding
GO:0019220-regulation of phosphate metabolic process	GO:0048770-pigment granule
GO:0042325-regulation of phosphorylation	GO:0051252-regulation of RNA metabolic process
GO:0044093-positive regulation of molecular function	hydrolase
GO:0051174-regulation of phosphorus metabolic process	lipoprotein
Ion transport/Channels	membrane
calcium	metal-binding
GO:0005509-calcium ion binding	mmu04062:Chemokine signaling pathway
GO:0042592-homeostatic process	mmu04670:Leukocyte transendothelial migration
GO:0048878-chemical homeostasis	mutagenesis site
Neuron	oxidoreductase
GO:0007610-behavior	phosphoprotein
GO:0030030-cell projection organization	receptor
GO:0030182-neuron differentiation	sequence variant
GO:0050877-neurological system process	signal
Cytoskeleton	signal peptide
GO:0005856-cytoskeleton	splice variant
GO:0043228-non-membrane-bounded organelle	topological domain:Cytoplasmic
GO:0043232-intracellular non-membrane-bounded organelle	topological domain:Extracellular
	transmembrane
	transmembrane region zinc